PAPER

Check for updates

DFT screening of metallic single-replacements for lead-free perovskites with intrinsic photovoltaic functionalities†

Clark Zhang [ID] and Xuan Luo [ID] *

Methylammonium lead triiodide perovskites, $CH_3NH_3PbI_3$ ($MAPbI_3$), are solution-processable materials with photovoltaic properties capable of surpassing those of silicon solar cells. However, concerns over lead toxicity and lack of exploration into transition metal perovskites drove this *ab initio* Density Functional Theory screening for environmentally friendly perovskite materials by incorporating transition and post-transition metals at the B-site of $MAPbI_3$. This revealed fourteen replacements to be suitable: their band structures are highly dispersive while band gaps of such materials fall within ideal ranges for single-junction and tandem cells. Transition metal monoreplacements are shown to be viable perovskites after reducing the size of the halide, corroborating that tunability of the band gap is observed in halide replacement at the X-site. Strong peaks in the imaginary output of the dielectric function below 3.5 eV indicate high sunlight absorption efficiency for select materials. Excellent carrier mobility is expected of studied materials as their effective mass is low. This work helps gain further insight into the viability of transition metals for lower toxicity and higher absorption divalent perovskites.

1 Introduction

In an effort to reduce the impact of global warming, renewable energy reliance has increased. Recent reductions in manufacturing costs of solar cells are steps towards the future use of large-scale photovoltaics cells (PV). However, cost and efficiency are still challenges faced by the PV industry. A new family of hybrid organic–inorganic lead halide perovskites offer high prospects on both energy conversion efficiency and production cost, especially methylammonium lead triiodide ($CH_3NH_3PbI_3$ or $MAPbI_3$).

$MAPbI_3$ has an extremely high absorption coefficient, long charge diffusion length, high defect tolerance, and high ambipolar transport. It has an experimental band gap of 1.55 eV,[1,2] close to that of the ideal band gap (which yields the highest theoretical conversion efficiency), 1.35 eV.[3] The outstanding performance of these materials proves useful for other optoelectronic applications.[4]

However, there are two main issues: the stability and the toxicity of lead (Pb). The presence of Pb in high performing perovskites poses serious environmental and health concerns. Solar cells are placed in direct contact with nature, so exposure to rainfall and solar heating is inevitable. Degradation into

volatile PbI_2 is highly likely due to the low thermal stability of $MAPbI_3$, causing severe chronic health problems.[5] Lead pollution further impacts natural resources, diffusing into the atmosphere, contaminating water sources, and emitting greenhouse gases.[6] Elimination of the Pb toxicity from perovskite cells requires complete replacement of Pb with other non-toxic elements.

The present study is a systematic search for stable methylammonium-metallic halide alternatives to Pb-based perovskites. Each suitable metal candidate was trialed as a single replacement of Pb at the B-site. Replacements of iodine at the X site with bromine were conducted for every B-site replacement, and with X-site replacement with chlorine for select perovskites. The paper details methods used to perform first-principles calculations, presents, discusses and compares results to other theoretical and experimental researches. The results show that proposed lead-free perovskite materials display heightened optoelectrical properties, greater stability, and much potential for use in single-junction and tandem solar cells.

2 Computational details

First-principles calculations were performed in the frame of Density Functional Theory (DFT) with the GGA-PBE exchange–correlation functional implemented in ABINIT[7] code. PAW pseudopotentials,[8] generated with the ATOMPAW code, were used to calculate the electronic structure of each perovskite, shown in Fig. 1. Originally, only 48 perovskites were to be

National Graphene Research and Development Center, Heming Avenue, Springfield, Virginia, USA

† Electronic supplementary information (ESI) available: PDOS and TDOS of $MAPbI_3$, studied band structures, and highlights in transition metal perovskite band gaps. See DOI: 10.1039/d0ra03034a
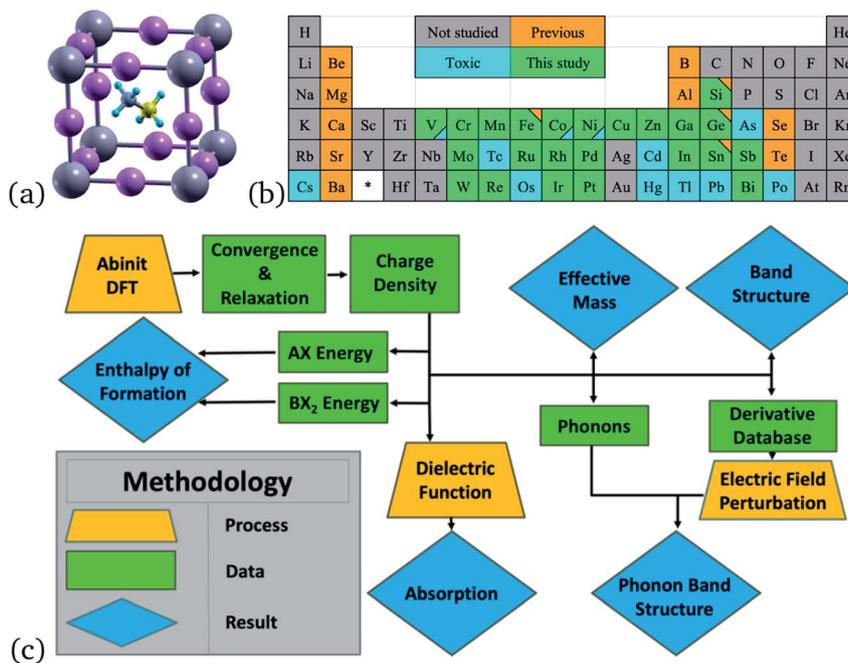
Fig. 1 (a) Unit cell of MAPbI$_3$ (ball and stick) from an isometric view, Pb represented in grey, I in pink, C in yellow, N in greyish blue, H in bright blue. (b) Elements used to replace lead at the B-site are colored green. Elements with Q3D Class 1 and 2A of toxicity[16] are colored blue. Previously studied elements for single-replacement of Pb are colored orange. Triangles in the corner represent two colorings. (c) A diagram of the research process and order of calculations used in this project. Orange trapezoids represent major calculations and processes. Green rectangles represent obtained data. Blue rhombuses represent final results.

considered, but MAZnCl$_3$ was later included after analyzing how the halogen tunability of the band gap affected the methylammonium zinc tribromide perovskite (see Section 3.1).

Convergence studies (see Fig. S1†) in the energy cutoff and the density of the k-mesh revealed 25 hartree and a density of 6 × 6 × 6 to be sufficiently converged. A homogenous shift in the grid of k-points of 0.5, 0.5, 0.5 (reduced coordinates in the coordinate system defining the k-point lattice) was implemented to increasing the calculation efficiency. Perovskites were relaxed to a pseudo-cubic crystal structure with the tolerance on the maximal force of 5×10^5 hartree per bohr and with a tolerance on the differences in forces per self-consistent cycle of 5×10^6 hartree per bohr. Dilation of primitive vectors was conducted with the Broyden–Fletcher–Goldfarb–Shanno minimization.[9–12]

For the band structure, k-points S, X, U, R, Γ, Z, T, and Y were selected as the circuit to sample the irreducible first Brillouin zone, taking into account spin–orbit coupling.

Effective mass was calculated using a linear response function that eliminates the need for spin–orbit coupling (SOC) and temperature smearing.[13] Degenerate bands were treated by using transport equivalent effective mass to avoid double perturbation.

For absorption, the Kohn–Sham band structure is further corrected using a one-shot G_0W_0 quasiparticle calculation[14] for solids with an energy cutoff of the wavefunction, sigma exchange, and a dielectric energy cutoff of 25 hartree (an exact treatment of the exchange part can be achieved with these parameters set to the value of the energy cutoff[15]). The lowest

occupied band considered was band number six, with a total of 44 bands for the Bethe–Salpeter calculation. This screening was formatted with an unsymmetrical k-mesh (shifted along the primitive axis by 0.11, 0.21, 0.31) and a 6 × 6 × 6 q-point mesh, and solved with Bethe–Salpeter equations. The imaginary output was plotted against light intensities from 0 to 4 eV, with intervals of 0.02 eV. The research process is depicted in Fig. 1c.

3 Results and discussion

3.1 Band structure

Table 1 shows the band gap values for MAPbI$_3$ and all monoreplacements in comparison to previous calculated results (with pseudo-cubic structures and without quasi-particle corrections) and experimental results. Several calculated band gaps in this study were reported with previously calculated and/or experimental results. All calculated band structures are displayed in the ESI,† with each band structure centered at the Fermi energy.

In general, the VB and CB dispersion is similar for most transition metals (see Tables S1 and S2†), especially the conduction band edge. In general, the VBM is dominated by the $5p_{x,y,z}$ orbitals of iodine while the CBM is dominated by the P orbitals in the B cation, see Fig. S2.† For certain monoreplacements, their metallic nature dwarfed the effects of methylammonium and iodine, resulting in a loss of the semiconductor properties of those materials.

Most transition metal monoreplacements didn't form any band gaps. However, MACuI$_3$ formed an indirect band gap with

Table 1 Methylammonium triiodide monoreplacement fundamental, optical, previous, experimental band gaps

Material	Fund. (eV)	Opt. (eV)	PBE prev. (eV)	Exp. (eV)
$MAPbI_3$	1.59	1.59	1.63,[1] 1.59 [17]	1.55 [18]
$MASiI_3$	1.70	1.70	0.14 [1]	—
$MAVI_3$	0.00	0.00	0	—
$MACrI_3$	0.00	0.00	—	—
$MAMnI_3$	0.00	0.00	—	—
$MAFeI_3$	0.00	0.00	—	—
$MACoI_3$	0.00	0.00	—	—
$MANiI_3$	0.00	0.00	—	—
$MACuI_3$	0.85	1.25	—	—
$MAZnI_3$	1.89	1.89	2.72 [1]	—
$MAGaI_3$	1.45	1.45	0.72 [1]	—
$MAGeI_3$	1.38	1.38	—	1.90 [1]
$MAMoI_3$	0.00	0.00	—	—
$MARhI_3$	0.00	0.00	—	—
$MARuI_3$	0.00	0.00	—	—
$MAPdI_3$	0.00	0.00	—	—
$MAInI_3$	0.61	0.61	—	—
$MASnI_3$	1.52	1.52	0.50 [1]	1.10 [1]
$MASbI_3$	0.00	0.00	—	—
$MAWI_3$	0.00	0.00	—	—
$MAReI_3$	0.00	0.00	—	—
$MAIrI_3$	0.00	0.00	—	—
$MAPtI_3$	0.00	0.00	—	—
$MABiI_3$	0.00	0.00	—	—

the VBM at point R and a CBM and point Z. $MAZnI_3$ formed a direct band gap of 1.89 eV at point R, see Fig. S5(4a).† Partial experimental replacement of Pb with Zn ($MAI[PbI_2]_{0.97}[ZnCl_2]_{0.03}$) shows heightened conversion efficiency of 1.8% compared to $MAPbI_3$.[19] This indicates ZnCl is a viable PV material, and its other properties are explored throughout this study.

The post-transition metal monoreplacement band gaps mostly fell between 1.3 and 1.7 eV. From group XIII elements, $MAGaI_3$ was studied by Ali *et al.*[1] and they found it to have a band gap of 0.72 eV, while this study finds it to be 1.45 eV. This discrepancy is attributed to the denser *k*-point mesh used in this study. Both the gallium and indium replacements had a single very high energy valance band (near the Fermi level) compared to the other valance bands (see Fig. S5(4b) and S6(5c),† respectively), therefore, their conversion efficiencies would be lower due to the energy expended during the phonon-assisted recombination.

Group XIV consists of Si, Ge, Sn, and Pb. $MASiI_3$ has the largest band gap of the group, at 1.70 eV. $MASnI_3$ has a band gap of 1.52 eV, however, differs from the previously reported results. $MAGeI_3$ is also a prospective alternative to $MAPbI_3$. It has an experimental band gap of 1.90 eV, larger than the calculated band gap of 1.38 eV. A binary mixture of Sn/Ge or with other suitable replacements could result in very strong absorption efficiencies.

Group XV consists of metalloids As and Sb, and poor metal Bi. Arsenic was not studied due to its toxicity. Both Sb and Bi monoreplacements have an intermediate band. This is interesting for intermediate band solar cells, but not for the current study, so group XV materials are not suitable for making a direct band gap material (Table 2).

Further replacement of the X triple anion was studied with bromine (X-site = Br).

Replacing iodine with lighter halogens increased the bandgap; methylammonium triiodide perovskites with direct band gaps had an increase in their band gap, much higher than the ideal band gap for single junction cells (1.35 eV), when the triiodide was replaced with tribromide. However, replacement of triiodide with tribromide opened up an optical band gap of some transition metal monoreplacements, indicating they have semimetal properties. This can be noted in $MAMnBr_3$, $MAFeBr_3$, and $MARuBr_3$. The VBM and CBM is shown in more detail in Fig. S3,† represented in yellow fill. This is crucial for further research into the incorporation of transition metals in PV materials.

After noting how $MAZnBr_3$ had a band gap of 1.49 eV, we decided to study $MAZnCl_3$ and $MAZnF_3$ as well because replacement at the X-site with a lighter halogen could result in another perovskite with a close-to-ideal band gap. As predicted, $MAZnCl_3$ had a band gap of 1.69 eV, shown in Fig. 2, but $MAZnF_3$ had a band gap of 3.55 eV. In all later sections, $MAZnCl_3$ is another perovskite that we studied and found the properties of. Its prospects as a new foundation for experimental PV investigations will be made clear as its properties are discussed in later sections.

No other trichloride materials were studied since the tunability nature of the band gap would increase the band gap

Table 2 Methylammonium tribromide monoreplacement fundamental, optical, previous, experimental band gaps

| Material	Fund. (eV)	Opt. (eV)	PBE prev. (eV)	Exp. (eV)
$MAPbBr_3$	2.23	2.23	2.1 [1]	2.3 [20]
$MASiBr_3$	2.57	2.57	—	—
$MAVBr_3$	0.00	0.00	—	—
$MACrBr_3$	0.00	0.00	—	—
$MAMnBr_3$	0.14	0.11	—	—
$MAFeBr_3$	0.12	0.08	—	—
$MACoBr_3$	0.00	0.00	—	—
$MANiBr_3$	0.00	0.00	—	—
$MACuBr_3$	3.74	3.74	—	—
$MAZnBr_3$	1.49	1.49	—	—
$MAGaBr_3$	1.85	1.85	—	—
$MAGeBr_3$	2.45	2.45	—	—
$MAMoBr_3$	0.00	0.00	—	—
$MARhBr_3$	0.00	0.00	—	—
$MARuBr_3$	0.19	0.18	—	—
$MAPdBr_3$	0.00	0.00	—	—
$MAInBr_3$	1.57	1.57	—	—
$MASnBr_3$	1.97	1.97	—	—
$MASbBr_3$	0.00	0.00	—	—
$MAWBr_3$	0.00	0.00	—	—
$MAReBr_3$	0.00	0.00	—	—
$MAIrBr_3$	0.00	0.00	—	—
$MAPtBr_3$	0.00	0.00	—	—
$MABiBr_3$	0.75	0.25	—	—
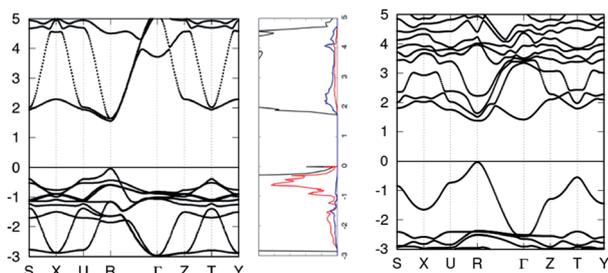
Fig. 2 Band structure with its TDOS and PDOS (iodine in red, lead in blue) of MAPbI$_3$ on the left and band structure of MAZnCl$_3$ on the right. The Fermi energies are shifted to be at 0 eV in the band structures.
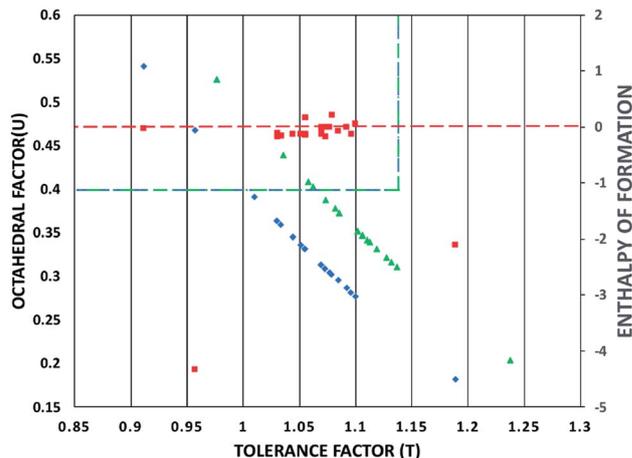

Fig. 3 The tolerance factor (t) and the octahedral factor (μ) (blue rhombic symbols) represent the structural stability for the studied triiodide perovskites, while the green triangles represent the structural stability for the studied tribromide perovskites. The red square symbols represent calculated enthalpies of formation in ΔH/f.u. The blue/green dotted lines represent the suitable range for the tolerance and octahedral factors. The red dotted line an enthalpy of formation of 0 eV/f.u.

of all trichloride monoreplacements beyond that of the ideal band gap. Therefore, studying them would be counterintuitive.

For monoreplacements, it can be concluded that Ge, Sn, Si, and Zn perovskites are the best replacements of Pb in MAPbI$_3$ for high performing solar cells. However, perovskites with band gaps inconsistent with the single-junction ideal can still be used in creation of tandem solar cells.[21,22]

3.2 Structural and thermal stability

A main issue of MAPbI$_3$ is its poor structural and thermal stability. According to Yang *et al.*[12] and Li *et al.*,[23] a material with Goldschmidt tolerance factor[24] between 0.81 and 1.11 exists in a cubic to pseudocubic (lattice parameters relatively equal; dihedral angles relatively close to 90°) perovskite structure. The octahedral factor (μ) further indicates severity of octahedral tilting, the primary factor for structural distortions; the suitable range for the octahedral factor is $0.4 \leq \mu \leq 0.90$.

$$t = \frac{r_A + r_X}{\sqrt{2}(r_B + r_X)} \quad \mu = \frac{r_B}{r_X} \qquad (1)$$

where $r_{A,B,X}$ represents the ionic radii[25] of each atom. For methylammonium, the atomic radius is the distance from the center of the C–N bond to the furthest edge of the N atom, yielding a value of 2.17 Å.

The thermal stability of each perovskite is determined *via* its energy of formation. MAPbI$_3$ is thermally unstable, decomposing into the compounds MAI + PbI$_2$ above 333 K.[26] Similarly, this study considers the decomposition of all mono-replacements in the form ABX$_3 \rightarrow$ AX + BX$_2$. The enthalpy of formation can be computed through the following equation:

$$\Delta H = E(ABX_3) - [E(AX) + E(BX_2)] \qquad (2)$$

where $E(x)$ represents the total energy of each perovskite. Since DFT calculations are performed at 0K, the enthalpy of formation calculated is a sign of stability. A table of all tolerance factors and enthalpies of formation can be found in Table S1.†

3.2.1 Triiodide perovskites. Calculated tolerance factors and enthalpies of formation for MAPbI$_3$ are consistent with previous results (-0.2 eV/functional unit (f.u., where one functional unit is a $1 \times 1 \times 1$ unit cell)). In Fig. 3, the tolerance factor (t) and octahedral factor (μ), and the enthalpy of formation of all monoreplacements are displayed in comparison to

MAPbI$_3$. Most monoreplacements fell within the acceptable range, MASiI$_3$ being the exception. The linear relationship between the tolerance factor and octahedral factor results in numerous transition metal replacements and the silicon replacement falls outside the suitable range for the Goldschmidt tolerance factor and octahedral tilting factor; only MAPbI$_3$ and MABiI$_3$ were tolerated. The octahedra as slightly offset to compensate for the large size of the iodine atom relative to the atom at the B-site. However, tilting of the octahedra didn't produce a significant negative effect on the other PV properties of the perovskites. Future research can explore doping the perovskite to reduce tilting and increase structural stability. Compared to MAPbI$_3$, most monoreplacements were

Table 3 Effective masses for electrons (e) and holes (h) in units of the free electron mass for select monoreplacements

Material	m_e	m_h	m_e (prev.)	m_h (prev.)
Si	0.20	0.15	0.19 [27]	0.16 [27]
MAPbI$_3$	0.18	0.24	0.19,[27] 0.30 [28]	0.25 [27]
MAGaI$_3$	0.24	0.18	—	—
MACuI$_3$	0.88	0.88	—	—
MAGeI$_3$	0.24	0.32	—	—
MAInI$_3$	0.45	0.14	—	—
MASnI$_3$	0.17	0.14	—	—
MAZnI$_3$	0.65	0.33	—	—
MAGaBr$_3$	0.30	0.60	—	—
MACuBr$_3$	0.73	0.73	—	—
MAGeBr$_3$	0.24	0.32	—	—
MAInBr$_3$	0.15	0.30	—	—
MASnBr$_3$	0.07	0.15	—	—
MABiBr$_3$	0.14	0.22	—	—
MAZnBr$_3$	0.61	0.21	—	—
MAZnCl$_3$	0.25	0.25	—	—

also marginally stable, with the exception of $MABiI_3$, with ΔH -4.23 eV/f.u., and $MASiI_3$, with ΔH -2.10 eV/f.u., which were much more thermally stable.

3.2.2 Tribromide and trichloride perovskites. Calculated tolerance factors and octahedral factors follow the same trend methylammonium triiodide perovskites did: a negative correlation, except shifted up due to the smaller effective ionic radius of iodine (I = 220 pm, Br = 196 pm). However, the lighter halogens, with smaller atomic radii, fit better with the smaller atomic radii of the transition metals. Based on these trends, a non-triiodide perovskite with a light replacement for lead is the most structurally stable. $MAZnCl_3$ exhibited -0.51 eV/f.u., or $\Delta H = -49.5$ kJ mol^{-1}, the third most negative enthalpy of formation of the perovskites tested (Table 3).

3.3 Effective mass

The effective mass of all, with the exception of bismuth, tin, and gallium monoreplacements, had isotropic effective masses of electrons and holes. $MABiBr_3$ has higher effective mass of holes/electrons along one primitive vector. The same effect is seen in $MASnI_3$, with 0.5 effective mass of electron along one primitive vector. Lastly, $MAGaBr_3$ has 1.5 effective mass of electrons along one primitive vector.

In general, m^* of most monoreplacements are higher than that of $MAPbI_3$ and of crystalline silicon cells. However, the tin monoreplacement performed exceptionally well, consistently achieving lower effective mass of holes and electrons than $MAPbI_3$ with both triiodide and tribromide. As triiodide is replaced with lighter halogens, the m^* was reduced. Based on these trends, the lighter the substance at the X-site leads to lower m^*.

$MAZnCl_3$ fits into the above trend well. The zinc triiodide, tribromide, and trichloride perovskites had decreasing effective masses. $MAZnCl_3$ has effective masses of electrons is comparable to that of conventional crystalline silicon PV materials while its effective mass of electrons is comparable to that of $MAPbI_3$.

3.3.1 Dielectric function. The absorption in this study is entirely dependent on the imaginary solution to the dielectric equation, as a function of energy of light, from 0 to 4 eV.

Therefore, only qualitative judgments on the absorption window and peak absorption can be made. It is calculated with the equation:

$$\varepsilon_2(\omega) = \frac{2e^2\pi}{\Omega\varepsilon_0} \sum_{\mathbf{k},\mathrm{v},\mathrm{c}} |\langle \psi_{\mathbf{k}}^{\mathrm{c}} | \hat{\mathbf{u}} \cdot \mathbf{r} | \psi_{\mathbf{k}}^{\mathrm{v}} \rangle|^2 \delta\left(E_{\mathbf{k}}^{\mathrm{c}} - E_{\mathbf{k}}^{\mathrm{v}} - \hbar\omega\right) \quad (3)$$

where ω is light frequency, and $\psi_{\mathbf{k}}^{\mathrm{c}}$ and $\psi_{\mathbf{k}}^{\mathrm{v}}$ are, respectively, the conduction band and valance band wave functions at $\mathbf{k}$ calculated with the GGA approach. The vector $\hat{\mathbf{u}}$ points along with the polarization of the effective electric field—for tested monoreplacements in comparison to $MAPbI_3$.

Ninety-eight percent of solar flux is below 3.4 eV,[22] concentrated towards infrared light, indicating that such materials with peak absorption below 3.4 eV are strongly efficient for PV applications.

The imaginary part of the dielectric function (ε_2) is displayed in Fig. S4† for select monoreplacements, compared to $MAPbI_3$. The $MAPbI_3$ results are comparable to those of previous DFT studies and of experimental results.[27,29] All of the selected monoreplacements display absorption peaks at energies lower than that of $MAPbI_3$ (below 2.5 eV). Secondary and higher order peaks appear in lead-free perovskites because there are fewer degenerate bands at critical points S, Q, R, Γ, and T.

Replacement of iodine with bromine shifted the strongest absorption peaks from between 1 eV to 1.8 eV, clustered around 1.75 eV, corresponding to 700 nm red light (in the center of the solar flux concentration). These two trends indicate that lighter halogens at the X-site and lighter monoreplacements at the B-site red-shift absorption towards the bulk of solar concentration, minimizing thermalization loss.

Fig. 4 displays the ε_2 of $MAPbI_3$ in comparison to the ε_2 of $MAZnCl_3$. $MAZnCl_3$ displayed similar absorption peaks to $MAPbI_3$: one strong absorption peak between 2 eV and 2.5 eV and a second absorption peak around 3 eV. This indicates $MAZnCl_3$ could have high conversion efficiencies for the same energies of light as $MAPbI_3$. Interestingly, $MAZnCl_3$ displayed its strongest absorption peak around 4 eV. Since energy peak is greater than most of the solar flux energy, $MAZnCl_3$ could find use in concentrator solar cells, where the incident energy is much higher.

4 Conclusions

This study presents a systematic DFT study exploring the possibility of monoreplacements of lead in $MAPbI_3$ with non-toxic metallic elements. For homogeneous single-junction solar cells, it can be determined that Ge, Sn, Si, and Zn are the best replacements of lead in $MAPbI_3$. However, incorporation of other transition metals is feasible with light anions at the X-site, due to the tunability of the band gap. Based on discussed trends, a perovskite with a relatively lighter replacement of lead at the B-site and a lighter anion at the X-site would maximize structural stability, carrier and hole mobility, and absorption efficiency. $MAZnCl_3$ fits this description well; it has a close-to-ideal band gap (1.69 eV), low effective mass (0.25 m^*), high structural stability ($t = 1.06$, $\mu = 0.52$), high thermal
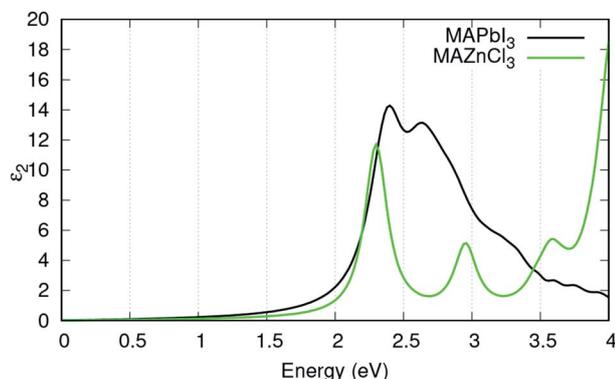

Fig. 4 Imaginary part of the calculated dielectric function, ε_2 of $MAPbI_3$ in black, $MAZnCl_3$ in green.

stability (ΔH -49.5 kJ mol^{-1}), and absorption similar to MAPbI$_3$. Zinc is also a highly abundant element in the Earth's crust, reducing production cost. MAZnCl$_3$, as well as the data and trends in this study, establishes a new foundation for experimental investigations in low cost, non-toxic, lead-free perovskites for photovoltaic applications.

Conflicts of interest

There are no conflicts to declare.

Acknowledgements

Notes and references

1 R. Ali, G.-J. Hou, Q.-B. Zhu, Z.-G. Yan, Q.-R. Zheng and G. Su, *Chem. Mater.*, 2018, **30**, 718–728.
2 M. Johnston and L. Herz, *Acc. Chem. Res.*, 2016, **49**, 146–154.
3 W. Shockley and H. J. Queisser, *J. Appl. Phys.*, 1961, **32**, 510–519.
4 N. Rathore, N. L. Panwar, F. Yettou and A. Gama, *Int. J. Ambient Energy*, 2019, 1–18.
5 A. Babayigit, A. Ethirajan, M. Muller and B. Conings, *Nat. Mater.*, 2016, **15**, 247–251.
6 J. Gong, S. B. Darling and F.-Q. You, *Energy Environ. Sci.*, 2015, **8**, 1953.
7 X. Gonze, B. Amadon, P.-M. Anglade, J.-M. Beuken, F. Bottin, P. Boulanger, F. Bruneval, D. Caliste, R. Caracas, M. Cote, T. Deutsch, L. Genovese, P. Ghosez, M. Giantomassi, S. Goedecker, D. Hamann, P. Hermet, F. Jollet, G. Jomard, S. Leroux, M. Mancini, S. Mazevet, M. Oliveira, G. Onida, Y. Pouillon, T. Rangel, G.-M. Rignanese, D. Sangalli, R. Shaltaf, M. Torrent, M. Verstraete, G. Zerah and J. W. Zwanziger, *Comput. Phys. Commun.*, 2009, **180**, 2582–2615.
8 P. Blochl, *Phys. Rev. B: Condens. Matter Mater. Phys.*, 1994, **50**, 17953–17979.
9 C. G. Broyden, *J. Inst. Math. Its Appl.*, 1970, **6**, 76.
10 R. Fletcher, *Comput. J.*, 1970, **13**, 317.
11 D. F. Shanno, *Math. Comput.*, 1970, **24**, 647.
12 D. Yang, X. Lv, J. Zhao, Q. Xu, Y. Fu, Y. Zhan, A. Zunger and L. Zhang, *Chem. Mater.*, 2017, **29**, 524–538.
13 J. Laflamme Janssen, Y. Gillet, S. PoncÃ̌, A. Martin, M. Torrent and X. Gonze, *Phys. Rev. B*, 2016, **93**, 205147.
14 M. Giantomassi, M. Stankovski, R. Shaltaf, M. GrÃijning, F. Bruneval, P. Rinke and G.-M. Rignanese, *Phys. Status Solidi B*, 2011, **248**, 275–289.
15 W. G. Aulbur, L. Jönsson and J. W. Wilkins, *Solid State Phys.*, 2000, **54**, 1–218.
16 *I. C. for Harmonisation of Technical Requirements for Pharmaceuticals for Human Use*, 2019.
17 G. Giorgi and K. Yamashita, *Nanotechnology*, 2015, **26**, 442001.
18 G. E. Eperon, S. D. Stranks, C. Menelaou, M. B. Johnston, L. M. Herz and H. J. Snaith, *Energy Environ. Sci.*, 2014, **7**, 982–988.
19 J. Jin, H. Li, C. Chen, B. Zhang, L. Xu, B. Dong, H. Song and Q. Dai, *ACS Appl. Mater. Interfaces*, 2017, **9**, 42875–42882.
20 P. P. Boix, S. Agarwala, T. M. Koh, N. Mathews and S. G. Mhaisalkar, *J. Phys. Chem. Lett.*, 2015, **6**, 898–907.
21 S. Bremner, C. Yi, A. Almansouri, I. Ho-Baillie and M. Green, *Sol. Energy*, 2015, **135**, 750–757.
22 C. Henry, *J. Appl. Phys.*, 1980, **51**, 4494.
23 C. Li, X. Lu, W. Ding, L. Feng, Y. Gao and Z. Guo, *Acta Crystallogr., Sect. B: Struct. Sci.*, 2008, **64**, 702–707.
24 H. KronmÃijller and S. Parkin, *Handbook of magnetism and advanced magnetic materials: Spintronics and magnetoelectronics.*, John Wiley & Sons, 2007.
25 J. A. Wasastjerna, *Soc. Sci. Fenn., Commentat. Phys.-Math.*, 1923, **1**, 1–25.
26 Q. Wang, Q. Dong, T. Li, A. Gruverman and J. Huang, *Adv. Mater.*, 2016, **28**, 6734–6739.
27 R. Ali, G.-J. Hou, Q.-B. Zhu, Z.-G. Yan, Q.-R. Zheng and G. Su, *J. Mater. Chem. A*, 2018, **6**, 9220–9227.
28 K. Wang, X. Liang, K. L. Anokhin, N. Gerasimov and P. A. Dremova, *Adv. Electron. Mater.*, 2015, **1**, 150089.
29 Y. Jiao, F. Ma, G. Gao, H. Wang, J. Bell, T. Frauenheim and A. Du, *RSC Adv.*, 2015, **5**, 82346–82350.